Available online at www.sciencedirect.com
SCIENCE DIRECT®
Journal of Sound and Vibration 282 (2005) 805–830
JOURNAL OF SOUND AND VIBRATION
www.elsevier.com/locate/jsvi

Bridge dynamic responses due to road surface roughness and braking of vehicle

S.S. Law*, X.Q. Zhu

Department of Civil and Structural Engineering, Hong Kong Polytechnic University, Kowloon, Hung Hom, Hong Kong

Received 8 September 2003; received in revised form 2 March 2004; accepted 15 March 2004
Available online 28 September 2004

Abstract

The dynamic behavior of a multi-span non-uniform continuous bridge under a moving vehicle is studied by considering the effect of interaction between the structure, the road surface roughness and the vehicle. The bridge is modeled as a multi-span continuous Benoulli–Euler beam with non-uniform cross-section on linear spring supports with large stiffness. The vehicle is modeled as a group of moving loads at a fixed spacing. Numerical simulation and laboratory tests were performed on a single-span and a two-span beam. The first span is found to exhibit smaller dynamic responses compared with the other spans for both constant speed vehicle and with vehicle braking due to the smaller initial conditions of the vehicle at entry of the span. Braking of the vehicle generates excitation forces covering a wide range of frequencies and this requires a large number of vibration modes for an accurate prediction on the responses. Since braking in one span would create response in different spans, a more correct definition of impact factor with vehicle braking should be based on a comparison of the maximum dynamic and static responses at the same span in which braking occurs.

1. Introduction

The problem of bridge vibration caused by a moving vehicle has been studied extensively in the past. The researches can generally be categorized under nine headings [1]: the effect of suspension

*Corresponding author. Tel.: +852-2766-6062; fax: +852-2334-6389.
E-mail address: cesslaw@polyu.edu.hk (S.S. Law).

0022-460X/$ - see front matter © 2004 Elsevier Ltd. All rights reserved.
doi:10.1016/j.jsv.2004.03.032

Nomenclature

$\rho A(x)$ mass per unit length of beam
$EI(x)$ flexural stiffness of the beam
$P_s(t)$ the interaction force between the moving vehicle and the bridge
$\hat{x}_s(t)$ location of the axle
$w(x,t)$ lateral deflection of the beam at time t and position x
$W_i(x)$ mode shape function of the ith mode
$q_i(t)$ ith modal coordinate
R number of supports
θ_1, θ_2 rotation at the centroid of the tractor and the trailer, respectively
$x_{c1}, x_{c2}, y_{c1}, y_{c2}$ vertical and horizontal displacements of the centroid of the tractor and trailer, respectively
a_i, b_1, b_2 vehicle dimension parameters
E Young's modulus
F_d the driving force of vehicle
T, U kinetic and potential energy, respectively, of the bridge–vehicle system
W work of the non-conservative forces of the bridge–vehicle system
J_1, J_2 rotational moments of inertia of the tractor and the trailer, respectively
m_i mass of each part of the vehicle
L the length of the beam
S_1, S_2 vehicle dimensions
z_1^c, z_2^c vertical displacements of the centroid of the tractor and the trailer, respectively, due to movement of the vehicle supports
M_b, K_b, C_b mass, stiffness, and damping matrices of the bridge
M_c, K_c, C_c mass, stiffness, and damping matrices of the vehicle system
F_b, F_c generalized forces of the bridge and the vehicle system
$d(x)$ the road surface roughness function
$d'(x)$ first derivative of $d(x)$
$W_i'(x), W_i''(x)$ first and second derivatives of $W_i(x)$
t_b braking rise time
$W_{Ui}(x)$ vibration mode of the uniform beam
$S_d(f)$ displacement PSD of the bridge surface roughness
f the spatial frequency (cycles/m)
f_0 the reference spatial frequency (cycles/m)
Δ distance interval between successive ordinates of the surface profile
θ_i ith set of independent random phase angles uniformly distributed between 0 and 2π
δ variational symbol
$f_{d\max}$ amplitude of the braking force
I_d, I_m impact factor from deflection and moment, respectively.

systems, road surface roughness, bridge span length, vehicle braking, axle spacing, gross vehicle weight, vehicle speed, unit mass of bridge and bridge damping. Many numerical methods have been developed to study the influence of different factors on the dynamic behavior of the bridge.

The bridge structure has been modeled with the finite element method using the beam element [2], grillage method [3,4], eight-node quadrilateral Kirchhoff plate/shell element and three-node Euler–Benoulli beam [1,5,6], plate elements [7], and as an assemblage of beam and plate elements [8].

The vehicle has been modeled with different degrees of complexity. The simplest model is a quarter truck vehicle model [9–11]. The other two common models are the two-dimensional models [2,8,12,13]; and the three-dimensional models [1,2,4–7,14].

Based on the above models, the bridge–vehicle system is divided into subsystems with an interface between the bridge and the vehicle. The equations of motion of the bridge and the vehicle are in general solved separately by an iterative procedure [15]. Henchi et al. [6] solves the

coupled equations of motion directly by the central difference method. Yang and Lin [16] and Yang and Yau [17] developed a vehicle–bridge interaction element, and the method can be used to solve the problem with a series of vehicles moving in the same direction.

Most of the published works are on vehicles moving at a constant speed, and few works have been found to investigate the bridge dynamic response with non-uniform vehicle speed. A redistribution of the axle load occurs when the vehicle is subjected to braking, and this causes a significant change in the dynamic response of the bridge. The resulting dynamic effect may exceed those allowed for in the current design practice. Kishan and Traill-Nash [18] studied the braking effect on the bridge response with the bridge deck idealized as a simply supported beam. Gupta and Traill-Nash [19] presented impact factors from braking of a two-axle vehicle on a single-span bridge deck using a ramped braking function. Mulcahy [14] presented the moment amplification factors from braking of a three-axle vehicle on a single-span bridge deck. Later Chompooming and Yener [8] discussed the effect of vehicle deceleration on the bridge dynamics. Since most of the modern bridges are non-uniform in cross-section, continuous and are of long span, the study on the response of this type of bridge under moving vehicles is important.

This paper reports on the study of a dynamic response of a multi-span continuous bridge under a moving vehicle by considering the effect of interaction between the road pavement roughness and the braking of the vehicle. The analysis is presented for a three-axle tractor–trailer vehicle and the bridge is modeled as a multi-span continuous Euler–Benoulli beam with non-uniform cross-section. The intermediate supports are modeled as linear springs with large stiffness. The mode shapes of this non-uniform beam are calculated basing on the Ritz method. The initial vehicle position at braking, the amplitude of the braking force, the braking rise time, initial vehicle speed, different road classes of the ISO standard [20], and their effects on the impact factors are discussed. A single-span uniform bridge and a three-span non-uniform continuous bridge are studied in the simulation. Laboratory verification using a single-span and a two-span beam under braking from a moving vehicle is also reported. The effects of the different factors on the impact factors particularly for the three-span bridge are discussed.

2. Vehicle and bridge models

A tractor–trailer vehicle is studied as a representative of modern freight vehicle. The model of a seven-degree-of-freedom (7-dof) tractor–trailer vehicle is shown in Fig. 1. The seven vertical dof's are denoted by y_i and those at the contact points between the wheels and the pavement are denoted by z_i. Each vehicle axle has its stiffness and damping from the suspensions denoted with subscripts 1, 2 and 3, and a tyre stiffness and damping denoted with subscripts 4, 5 and 6. The mass of each axle assembly is denoted by m_3, m_4 and m_5 and that of the tractor and trailer are m_1 and m_2, respectively.

The bridge superstructure is modeled as a non-uniform continuous Euler–Bernoulli beam as shown in Fig. 2 with $(R-1)$ intermediate vertical point supports. This model is representative of a modern bridge superstructure which is usually non-uniform and continuous. $\{P_s(t), s = 1, 2, 3\}$ are the axle forces from the moving vehicle. The force locations are denoted by $\hat{x}_s(t), (s = 1, 2, 3)$ measured from the left support. The motion of the centroids of the tractor and trailer can then be

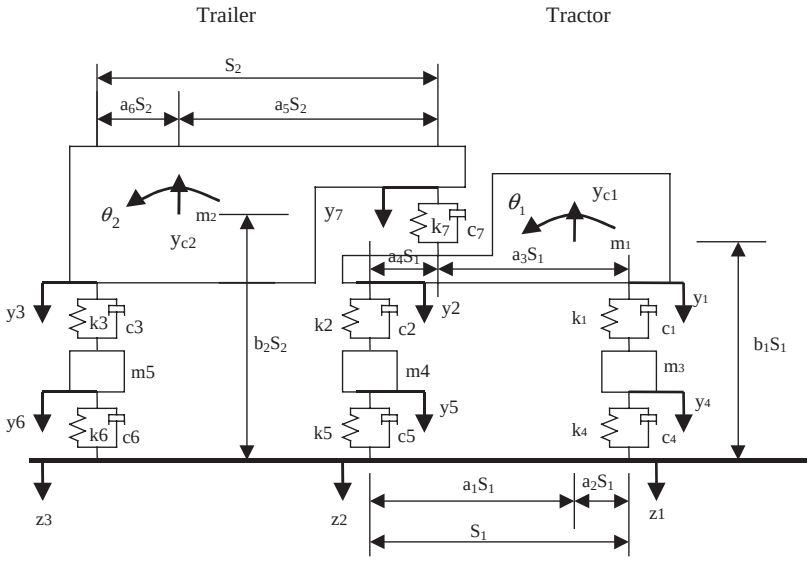

Fig. 1. Model of a seven degree-of-freedom vehicle.

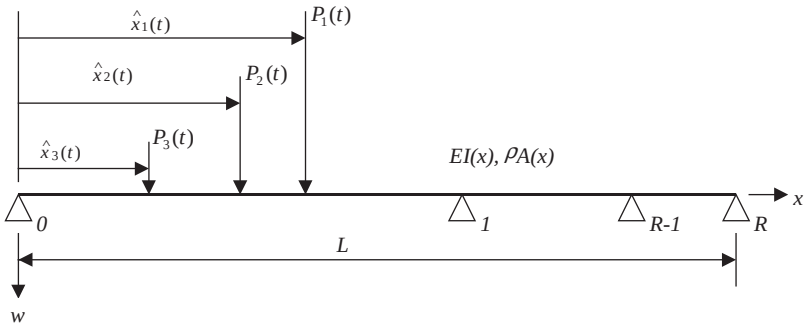

Fig. 2. A continuous beam with $(R-1)$ intermediate point supports under the moving vehicle.

expressed in terms of the seven dof's of the vehicle model and the co-ordinates at the contact points between the bridge and the vehicle.

2.1. Vehicle-bridge interaction

The vertical displacements and rotations of the vehicle are relative to the static equilibrium position, and the coordinates z_i are measured from the static equilibrium position without the vehicle. The tyres are assumed to remain in contact with the bridge surface at all times. The intermediate supports are modeled as vertical linear springs with large stiffness to simulate bridge piers which are practically not perfectly rigid. The horizontal direction of the intermediate

supports is not restrained. The kinetic energy T and the potential energy U of the vehicle–bridge system can be obtained as

$$
\begin{aligned}
T &= T_b + T_c \\
&= \frac{1}{2}\int_0^L \rho A(x)\left(\frac{\partial w(x,t)}{\partial t}\right)^2 \mathrm{d}x + \tfrac{1}{2}m_1\dot{y}_{c1}^2 + \tfrac{1}{2}J_1\dot{\theta}_1^2 + \tfrac{1}{2}m_2\dot{y}_{c2}^2 \\
&\quad + \tfrac{1}{2}J_2\dot{\theta}_2^2 + \tfrac{1}{2}m_3\dot{y}_4^2 + \tfrac{1}{2}m_4\dot{y}_5^2 + \tfrac{1}{2}m_5\dot{y}_6^2 + \frac{1}{2}\sum_{i=3}^{5} m_i\dot{\hat{x}}_s(t)^2 + \tfrac{1}{2}m_1\dot{x}_{c1}^2 + \tfrac{1}{2}m_2\dot{x}_{c2}^2 \\
U &= U_b + U_c \\
&= \frac{1}{2}\int_0^L EI(x)\left(\frac{\partial^2 w(x,t)}{\partial x^2}\right)^2 \mathrm{d}x + \tfrac{1}{2}k_s\sum_{i=1}^{R-1} w(x_i,t)^2 + \tfrac{1}{2}k_1(y_1-y_4)^2 + \tfrac{1}{2}k_2(y_2-y_5)^2 + \tfrac{1}{2}k_3(y_3-y_6)^2 \\
&\quad + \tfrac{1}{2}k_7(y_7 - a_3y_2 - a_4y_1)^2 - m_1gz_1^c - m_2gz_2^c - m_3gz_1 - m_4gz_2 - m_5gz_3,
\end{aligned} \tag{1}
$$

where subscripts c and b denote the contributions from the vehicle and the bridge, respectively; ρ is the density of material of the bridge; $A(x)$ is the cross-sectional area; E is Young's modulus; $I(x)$ is the moment of inertia of the beam cross-section; $w(x,t)$ is the vertical displacement of the beam; x_i $(i = 0, 1, 2, \ldots, R)$ are the coordinates of intermediate point supports and end supports, k_s is the stiffness of the linear spring at the point constraints. y_{c1} and y_{c2} are the vertical displacements and x_{c1} and x_{c2} are the horizontal locations of the centroids of the tractor and the trailer, respectively, with subscripts 1 and 2 denoting the tractor and the trailer, respectively. J_1 and J_2 are the rotational moments of inertia of the tractor and the trailer, respectively, and g is the acceleration due to gravity. The bridge is assumed in equilibrium under its own weight before the vehicle enters the deck.

By separation of variables, the vertical displacement of the beam $w(x,t)$ can be expressed as

$$
w(x,t) = \sum_{i=1}^{n} q_i(t)W_i(x), \quad \{i = 1, 2, \ldots, n\}, \tag{2}
$$

where $\{W_i(x),\ i = 1, 2, \ldots, n\}$ are the assumed vibration modes that satisfy the boundary conditions and $\{q_i(t),\ i = 1, 2, \ldots, n\}$ are the modal coordinates of the bridge.

The motion of the vehicle is defined by the vehicle coordinates $\hat{x}_s(t)$ and y_i with the vehicle moving from left to right. The longitudinal position of the centroids x_{c1} and x_{c2} of the tractor and trailer, respectively, and the axle locations $\hat{x}_s(t), (s = 1, 2, 3)$ are relative to the bridge entry. The longitudinal position and the vertical displacement of the centroids of the tractor and trailer are, respectively,

$$
\begin{aligned}
x_{c1} &= \hat{x}_1(t) - a_1S_1 - b_1S_1\theta_1, \\
x_{c2} &= \hat{x}_1(t) - a_3S_1 - b_1S_1\theta_1 - a_5S_2 - b_2S_2\theta_2, \\
y_{c1} &= a_2y_1 + a_1y_2, \\
y_{c2} &= a_5y_3 + a_6y_7
\end{aligned} \tag{3}
$$

and the rotational deformations θ_1 and θ_2 of the centroids of the tractor and the trailer are, respectively,

$$\begin{aligned}\theta_1 &= (y_1 - y_2)/S_1,\\ \theta_2 &= (y_7 - y_3)/S_2.\end{aligned} \tag{4}$$

The vertical displacements of the centroids of the tractor and the trailer due to the motion of the vehicle relative to the contact points with the pavement are, respectively,

$$\begin{aligned}z_1^c &= a_2 z_1 + a_1 z_2,\\ z_2^c &= a_6(a_4 z_1 + a_3 z_2) + a_5 z_3.\end{aligned} \tag{5}$$

The work done by the system of non-conservative forces of the bridge-vehicle system can then be written as

$$\begin{aligned}W &= W_b + W_d + W_a + W_c\\ &= Q^{\mathrm{T}} C_b \dot{Q} + Y^{\mathrm{T}} C_c \dot{Y} + F_d \hat{x}_s(t) - P_1(t)(z_1 - y_4) - P_2(t)(z_2 - y_5) - P_3(t)(z_3 - y_6),\end{aligned} \tag{6}$$

where W_b, W_d, W_a, W_c are the work done by the damping force of the bridge, the driving force of the vehicle, the interaction forces, and the damping force of the vehicle, respectively. $Q = \{q_1(t), q_2(t), \ldots, q_n(t)\}^{\mathrm{T}}$ is the vector of modal coordinates of the bridge, F_d is the longitudinal drive force of the vehicle, C_c, C_b are the damping coefficient matrices of the vehicle and the bridge respectively. $\{P_1(t), P_2(t), P_3(t)\}$ are the interaction forces between the vehicle and the bridge written as

$$\begin{aligned}P_1(t) &= k_4(y_4 - z_1) + c_4(\dot{y}_4 - \dot{z}_1),\\ P_2(t) &= k_5(y_5 - z_2) + c_5(\dot{y}_5 - \dot{z}_2),\\ P_3(t) &= k_6(y_6 - z_3) + c_6(\dot{y}_6 - \dot{z}_3).\end{aligned} \tag{7}$$

Sharp change in the road surface causes local changes in the profile acting at the base of the tyre spring. Mulcahy [14] developed a 'tyre enveloping' model on the road surface roughness in which the profile is approximated by a quadratic parabola. This tends to smooth out the excitation from changes in the road profile. In the present study, the vertical displacements, z_i, at the points of contact of the wheels and the bridge are given below including the road surface roughness function $d(x)$ along the horizontal direction (the relation of function $d(x)$ to the road roughness definition will be given later):

$$\begin{aligned}z_i &= w(\hat{x}_i(t), t) + d(\hat{x}_i(t)) \quad (i = 1, 2, 3),\\ \dot{z}_i &= v\left.\frac{\partial w(x,t)}{\partial x}\right|_{x=\hat{x}_i(t)} + \left.\frac{\partial w(x,t)}{\partial t}\right|_{x=\hat{x}_i(t)} + v\left.\frac{\partial d(x)}{\partial x}\right|_{x=\hat{x}_i(t)} \quad (i = 1, 2, 3),\end{aligned} \tag{8}$$

where v is the horizontal velocity of the moving vehicle. Since $d(x)$ is independent of x, the last term in $\dot{z}_i$ can be equal to zero. The longitudinal position of the second and the third axles are related to that of the first as

$$\begin{aligned}\hat{x}_2(t) &= \hat{x}_1(t) - S_1,\\ \hat{x}_3(t) &= \hat{x}_1(t) - a_3 S_1 - a_5 S_2.\end{aligned} \tag{9}$$

Mulcahy [14] has presented the equation of motion for a three-axle vehicle on a single-span bridge using the Lagrange approach. The equation of motion of a three-axle vehicle on a multi-span bridge is presented in this paper using the Hamilton principle.

$$\int_{t_1}^{t_2} \delta(T - V + W)\,\mathrm{d}t = 0 \tag{10}$$

The equation of motion of the vertical motion of the vehicle–bridge system can be obtained in both y_i and q_i coordinates as

$$\begin{aligned} M_c\ddot{Y} + C_c\dot{Y} + K_c Y &= F_c, \\ M_b\ddot{Q} + C_b\dot{Q} + K_b Q &= F_b, \end{aligned} \tag{11}$$

where $Y = \{y_1, y_2, \ldots, y_7\}^{\mathrm{T}}$ is the vector of displacements at the seven dof's of the vehicle, F_c and F_b are vectors of generalized forces acting on the vehicle and the bridge structure, respectively. M_c, K_c, C_c and M_b, K_b, C_b are the mass, stiffness and damping matrices of the vehicle and beam, respectively. All terms in the equation are referred to in Appendix A.

The equation of motion of the horizontal motion of the vehicle in $\hat{x}_s(t)$ coordinate can also be written as

$$\begin{aligned} &\sum_{i=3}^{5} m_i\ddot{\hat{x}}_s(t) - (m_1 + m_2)b_1(\ddot{y}_1 - \ddot{y}_2) - m_2 b_2(\ddot{y}_7 - \ddot{y}_3) \\ &\quad = F_d + \sum_{s=1}^{3}\left[\sum_{i=1}^{n} W_i'(\hat{x}_s(t))q_i(t)\right] P_s'(t) \end{aligned} \tag{12}$$

where $P_s'(t)$ is referred to in Appendix A and

$$W_s'(\hat{x}_s(t)) = \left.\frac{\partial W_i(x)}{\partial x}\right|_{x=\hat{x}_s(t)} \quad (i = 1, 2, \ldots, n;\ s = 1, 2, 3). \tag{13}$$

The above formulation on the equations of motion of the bridge–vehicle system can be simplified for a two-axle vehicle by setting to zero the parameters associated with the trailer and eliminating from the equations of motion the corresponding dof's. The two-axle vehicle then corresponds to the tractor of the three-axle model. This modified model will be used in the experimental verification of the proposed method.

3. Mode shapes of the bridge deck

Mode shapes of the bridge deck are required in the solution of Eq. (2). The Ritz method is applied to solve for the beam vibration motions. For a single span simply supported beam with uniform cross-section, the vibration mode shapes are

$$W_{U_i}(x) = \sin\left(\frac{i\pi x}{L}\right) \quad (i = 1, 2, \ldots, n), \tag{14}$$

where n is the number of vibration modes. The vertical displacement of the beam can be assumed as a combination of these mode shapes satisfying the boundary conditions of the non-uniform beam as

$$W(x) = \sum_{i=1}^{r} b_i W_{U_i}(x), \tag{15}$$

where $\{b_i, i = 1, 2, \ldots, r\}$ is a set of constant coefficients. The problem is to find these coefficients by minimizing the following integral:

$$Z = \int_0^L \left[EI(x)(W''(x))^2 - \omega^2 \rho A(x)(W(x))^2 \right] \mathrm{d}x \tag{16}$$

to have

$$(K' - \omega^2 M)b = 0, \tag{17}$$

where K' and M are $n \times n$ matrices with their components k'_{jj} and m_{jj} given in Eq. (18), and $b = \{b_1, b_2, \ldots, b_n\}$ is an $n \times 1$ vector.

$$\begin{aligned} k'_{ij} &= \int_0^L EI(x) W''_{Ui}(x) W''_{Uj}(x)\, \mathrm{d}x \\ m_{ij} &= \int_0^L \rho A(x) W_{Ui}(x) W_{Uj}(x)\, \mathrm{d}x \end{aligned} \qquad (i = 1, 2, \ldots, n;\ j = 1, 2, \ldots, n). \tag{18}$$

Rewrite Eq. (17) as

$$(D - \omega^2 I)b' = 0 \tag{19}$$

and solving, we have

$$D = K'\, M^{-1}, \quad b' = Mb, \tag{20}$$

where ω^2 and b' are the eigenvalues and the eigenvectors of the matrix D. The vertical displacement of the beam $W(x)$ can then be obtained from Eq. (15).

4. Road surface roughness

The randomness of the road surface roughness can be represented with a periodic modulated random process. In ISO-8608 [20] specifications, the road surface roughness is related to the vehicle speed by a formula between the velocity power spectral density (PSD) and the displacement PSD. The general form of the displacement PSD of the road surface roughness is given as

$$S_d(f) = S_d(f_0) \cdot (f/f_0)^{-a}, \tag{21}$$

where $f_0 (= 0.1$ cycles/m) is the reference spatial frequency, a is an exponent of the PSD, and f is the spatial frequency (cycles/m). Eq. (21) gives an estimate on the degree of roughness of the road from the value of $S_d(f_0)$. This surface roughness classification is based on a constant vehicle velocity PSD and taking a equals to 2.

The road surface roughness function $d(x)$ in the time domain can be simulated by applying the inverse fast fourier transformation on $S_d(f_i)$ to give [6]

$$d(x) = \sum_{i=1}^{N} \sqrt{4S_d(f_i)\Delta f}\cos(2\pi f_i x + \theta_i), \tag{22}$$

where $f_i = i\Delta f$ is the spatial frequency, $\Delta f = 1/(N\Delta)$, Δ is the distance interval between successive ordinates of the surface profile, N is the number of data points, and θ_i is a set of independent random phase angles uniformly distributed between 0 and 2π.

5. Procedure of implementation

The coupled equations of motion of the bridge-vehicle system presented in Eqs. (11) and (12) are subjected to the compatibility constraints on the interaction forces and the displacements of the two sub-systems. The procedure to solve the problem is implemented as follows:

Step 1: The mode shapes $W_i(x)$ of the non-uniform multi-span continuous bridge deck are calculated from Eq. (17) to (20).

Step 2: Determine the mass, stiffness and damping matrices of both the vehicle and the bridge deck.

Step 3: Calculate the road surface roughness function $d(x)$ from Eq. (22) according to the selected road class in ISO-8608 [20].

Step 4: The responses of the bridge and vehicle are calculated by the Newmark method. The time step, parameters of Newmark method and the error for convergence are determined before the iteration. Set the initial values of Q and Y.

Step 5: Determine the initial vehicle position on the bridge deck.

Step 6: Calculate the excitation force on vehicle, F_c, and solve for the motion of the vehicle, Y, at time t from Eqs. (11) and (12).

Step 7: Calculate the excitation force on the bridge, F_b, and solve for the motion of the bridge, Q, at time t from Eq. (11).

Step 8: Solve for the displacement of the bridge $w(x,t)$ from Eq. (2).

Step 9: Repeat Steps 6–8 using the calculated Q and Y. Check the convergence of the difference between the two successively calculated $w(x,t)_i$ and $w(x,t)_{i+1}$.

$$\left\| w(x,t)_{i+1} - w(x,t)_i \right\| \leq \text{tolerance error.} \tag{23}$$

Step 10: If convergence is not achieved, repeat Steps 6–9. If convergence is achieved, repeat Steps 5–10 for the next time step.

6. Numerical study

The three-axle tractor-trailer vehicle shown in Fig. 1 is used in the study. The properties of the vehicle are physically measured [14] and they are as follows.

The body masses are

$$m_1 = 3930\ \text{kg}, \quad m_2 = 15{,}700\ \text{kg}, \quad m_3 = 220\ \text{kg}, \quad m_4 = 1500\ \text{kg}, \quad m_5 = 1000\ \text{kg}.$$

The vertical stiffness at each dof is

$$k_1 = 2.00 \times 10^6\ \text{N/m}, \quad k_2 = 4.60 \times 10^6\ \text{N/m}, \quad k_3 = 5.00 \times 10^6\ \text{N/m}, \quad k_4 = 1.73 \times 10^6\ \text{N/m},$$
$$k_5 = 3.74 \times 10^6\ \text{N/m}, \quad k_6 = 4.60 \times 10^6\ \text{N/m}, \quad k_7 = 2.00 \times 10^6\ \text{N/m}$$

and their respective viscous damping constants are

$$c_1 = 5000\ \text{N·s/m}, \quad c_2 = 30{,}000\ \text{N·s/m}, \quad c_3 = 40{,}000\ \text{N·s/m}, \quad c_4 = 1200\ \text{N·s/m},$$
$$c_5 = 3900\ \text{N·s/m}, \quad c_6 = 4300\ \text{N·s/m}, \quad c_7 = 5000\ \text{N·s/m}.$$

The axle spacing and the pitching moment of inertia of the tractor and the trailer are respectively,

$$S_1 = 3.66\ \text{m}, \quad S_2 = 6.20\ \text{m}, \quad J_1 = 1.05 \times 10^4\ \text{kgm}^2, \quad J_2 = 1.47 \times 10^5\ \text{kgm}^2.$$

The parameters on the dimensions of the vehicle are

$$a_1 = 0.5, \quad a_2 = 0.5, \quad a_3 = 1.0, \quad a_4 = 0.0, \quad a_5 = 0.58, \quad a_6 = 0.42, \quad b_1 = 0.25, \quad b_2 = 0.40.$$

Initially, both the vehicle and bridge are assumed to be at rest and the vehicle is traveling forward at a uniform velocity. A ramp function is assumed for the braking force [19]. This is based on the test results on highway vehicles conducted by the Transport and Road Research Laboratory, England, in 1975. The braking force increases linearly to a maximum $F_{d\max}$ and then stays constant until the vehicle either comes to a stop or crosses the bridge span and is written as

$$F_d = \begin{cases} -F_{d\max} t/t_b, & t < t_b, \\ -F_{d\max}, & t \geq t_b, \end{cases} \tag{24}$$

where t_b is the braking rise time.

The impact factors I_d and I_m calculated from the mid-span deflections and bending moments are defined, respectively, as

$$I_d = \frac{w_{\text{dynamic}}}{w_{\text{static}}}, \qquad I_m = \frac{B_{\text{dynamic}}}{B_{\text{static}}}, \tag{25}$$

where $w_{\text{dynamic}}, w_{\text{static}}, B_{\text{dynamic}}$ and B_{static} are the dynamic and static maximum deflections and bending moments at mid-span of the beam. w_{static} and B_{static} are obtained from an analysis with the vehicle crossing the bridge deck at a crawling speed.

Example 1. (A Uniform Single-Span Bridge Deck). No reference can be found in the literature on the use of non-uniform beam model in simulation studies, and hence the simply supported bridge deck studied by Mulcahy [14] is adopted for comparison. It is 32.6 m long with 16 m effective width, and the mass per unit area is 1240 kg/m^2. The flexural stiffness of the bridge superstructure is 4.592×10^{10} N m^2. The vehicle to bridge mass ratio is 0.0346. It is modeled as a simply supported uniform beam. The first 10 modes are used in the solution of the equation of motion in Eq. (11) and (12). A time step of 0.008 s is used in the integration, and it is approximately

one-tenth of the highest natural frequency of the bridge superstructure included in the analysis. This small time step is essential because braking produces an impulsive force that consists of frequency components over a wide spectrum.

The three-axle vehicle described previously is traveling at 17 m/s and it brakes at one-quarter span. The impact factors from mid-span bending moments and deflections are studied with variations in the following parameters:

(a) amplitude of the braking force ($F_{d\max} = 0.6m_cg$, $0.4m_cg$, $0.2m_cg$), where m_cg is the vehicle static weight;
(b) braking rise time, t_b= 0.6, 0.3 and 0.0 s;
(c) braking position of the vehicle;
(d) vehicle horizontal moving velocity; and
(e) different classes of road with the road surface roughness as specified in the ISO-8608 [20]. Road Classes A to E are used in the study.

The maximum impact factors computed for different braking force and braking locations are plotted in Figs. 3 and 4 with no surface roughness included in the analysis. These factors are the maximum values for the duration when the vehicle is on top of the bridge deck. The maximum impact factors for different classes of roads are presented in Table 1. The following observations are made:

(a) Fig. 3 shows that the variation of braking force $F_{d\max}$ has little effect on the maximum impact factor which is around 1.0 for all the magnitudes of braking force under study.

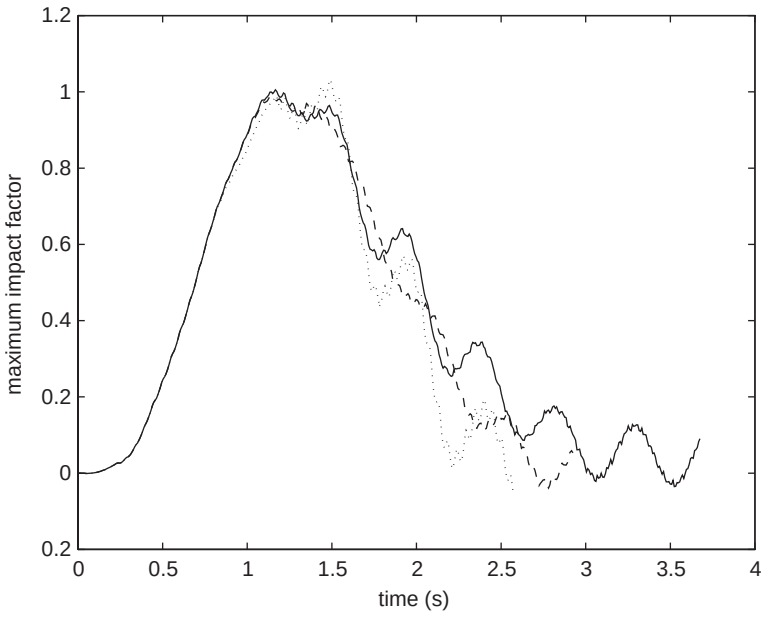

Fig. 3. Midspan impact factor from moment with different braking force at 1/4 span (—$0.6m_cg$; - - - $0.4m_cg$; $\cdots 0.2m_cg$).

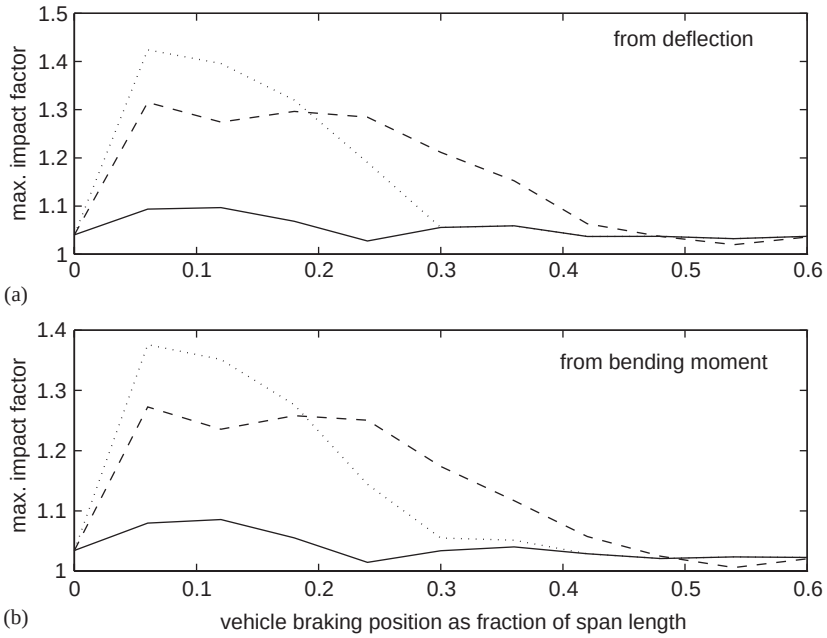

Fig. 4. Maximum impact factor from different vehicle braking position (— 0.6; - - - 0.3; ··· 0.0 s).

Table 1
Impact factors with different road surface conditions (single-span bridge deck)

Road class		A	B	C	D	E
1.7 m/s no braking	Deflection	1.09	1.06	1.14	1.24	1.79
	Moment	1.08	1.05	1.12	1.22	1.71
17 m/s no braking	Deflection	1.04	1.05	1.13	1.27	1.55
	Moment	1.04	1.04	1.10	1.23	1.49
17 m/s braking at 1/4 span	Deflection	1.08	1.17	1.32	1.62	2.24
	Moment	1.07	1.15	1.29	1.59	2.20

(b) Fig. 4 shows that the duration of braking rise time t_b has a very significant effect on the maximum impact factor, and braking within the first quarter span produces large impact factor compared with braking at other locations of the span. The impact factors produced from a hard braking $t_b = 0.3$ s. is approximately 1.30 while that from a sharp braking with $t_b = 0.0$ s. is approximately 1.42.

(c) Braking on the approach is not studied. Braking on the approach produces non-zero initial displacement and velocity of the vehicle at the entry point of the bridge, but the equivalent impulsive force from braking does not act on the bridge span. The dynamic effect depends on the characteristics of the vehicle suspension system, but it would be less severe than braking inside the bridge span in general.

(d) Table 1 shows the maximum impact factor for different road surface conditions when the vehicle is moving at 1.7 and 17 m/s or braking with a braking force of $0.6m_cg$ at a rise time of 0.6 s at one-quarter span. There is only slight difference in the impact factor for the cases traveling at constant velocity on Classes A–D roads. Also braking causes a distinctly higher impact factor when compared with the no braking cases on Classes C–E roads. Road Class E exhibits the worst dynamic responses with or without braking.

(e) The case of traveling at low velocity on Class E road has a significantly higher impact factor than that with a higher velocity. When the road roughness peaks are defined over a long time interval (lower speed), the vehicle would experience a lower frequency excitation closer to its own natural frequency, thus generating larger excitation force and larger dynamic responses in the bridge deck.

Example 2. (A Three-Span Continuous Non-Uniform Bridge Deck). A modern non-uniform three-span box-section bridge deck [21] shown in Fig. 5 is modeled as a 36 m-48 m-36 m three-span non-uniform continuous beam. The intermediate support stiffness is 10^9 N/m. It is noted that too large a stiffness value would cause ill-condition in the solution of the problem. The vehicle to bridge mass ratio is 0.0235. The time step required in the calculation of responses is taken as 0.0147 s taking into account the first ten modes of the bridge superstructure in the analysis. The mode shape function for the continuous beam is referred to [22]. The same three-axle vehicle is used in the study.

The dynamic effects are studied with variations in the influencing parameters for comparison. The maximum impact factors are plotted in Figs. 6–9 and 11, and the maximum impact

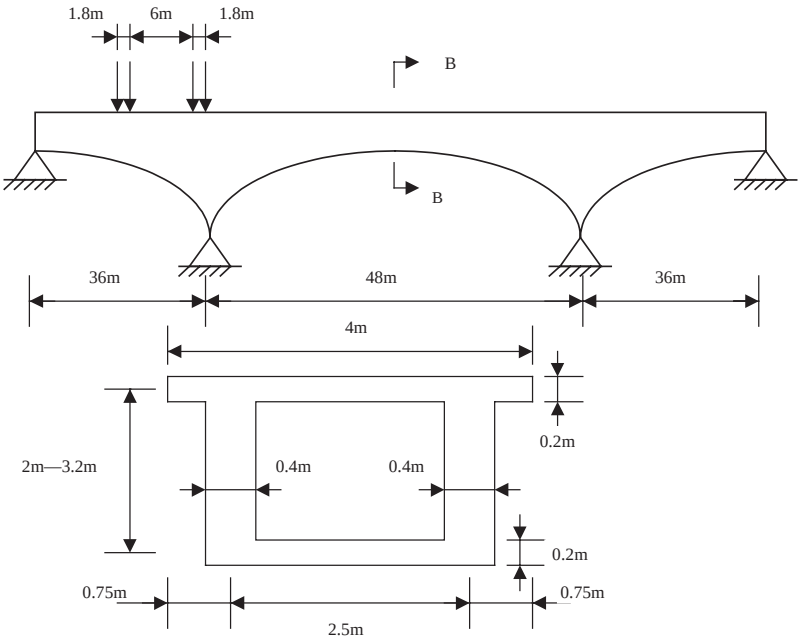

Fig. 5. A three-span continuous bridge.

factors for different classes of roads are shown in Tables 2 and 3. The following observations are made:

(a) Fig. 6 shows that the maximum impact factors at the mid-span of each of the three spans for different constant travelling velocities as a reference. No road surface roughness is included in the analysis. The impact factors are generally small even at high velocities. The impact factor is smallest in the second span among the three spans. This may be due to its higher flexibility compared with the other two spans.

(b) Fig. 7 shows the time histories of the impact factors resulting from braking at positions 2/7, 3/7 and 4/7 of the total bridge span, L, with $2/7L$ almost on the second support, and $3/7L$ and $4/7L$ are inside the second span. The vehicle initial velocity is 17 m/s, and Class B road is considered. The vehicle braking force $F_{d\,\max}=0.6m_cg$ and the braking rise time $t_b=0.6$ s. The impact factor from the second span is largest for these braking locations among the three spans. The impact factors are in general small with the highest value of 1.04 for braking at 3/7 span.

(c) Fig. 8 shows the time histories of impact factor from the vehicle braking at $3/7L$ on a Class B road moving with an initial velocity of 17 m/s. The braking rise time t_b is found to have a significant effect on the impact factor with a value of 1.17 for a hard braking at $t_b=0.3$ s. In the case of a sharp braking at $t_b=0.0$ sec., the impact factor is 1.49. It is noted that the oscillating component in the responses in Figs. 7–9 is due to the large pitching action of the vehicle arising from braking.

(d) Fig. 9 shows the time histories of impact factor at the middle of the second span from braking at $1/3L$ (within the second span) on a Class B road with an initial velocity of 17 m/s. The

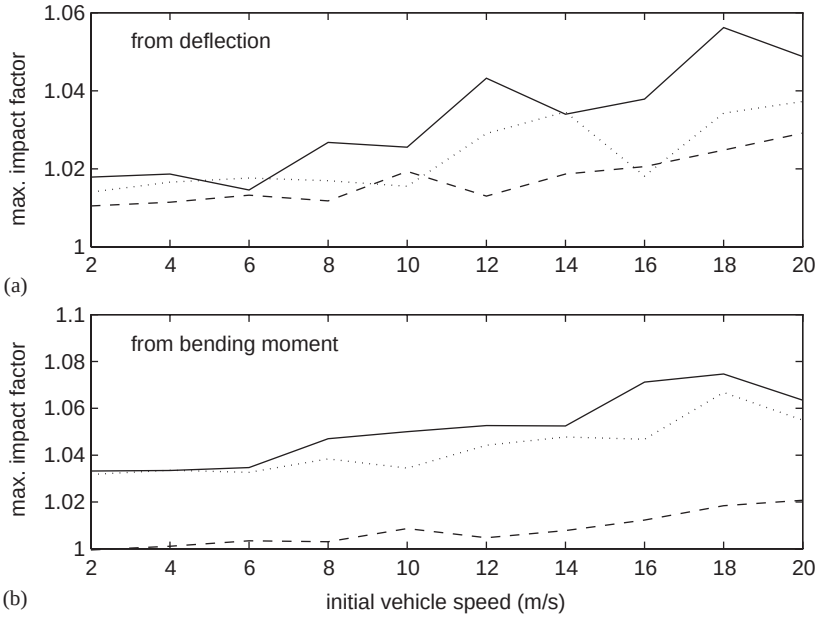

Fig. 6. Mid-span impact factor from different vehicle speed) (— first span; - - - second span; ⋯ third span).

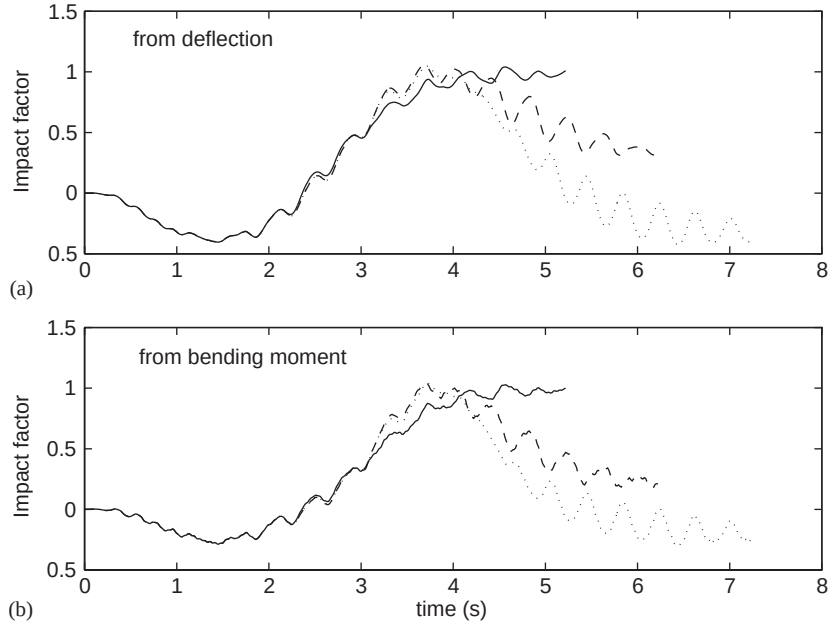

Fig. 7. Impact factor at middle of second span from different braking position (braking at: — $2/7L$; - - - $3/7L$; ⋯ $4/7L$).

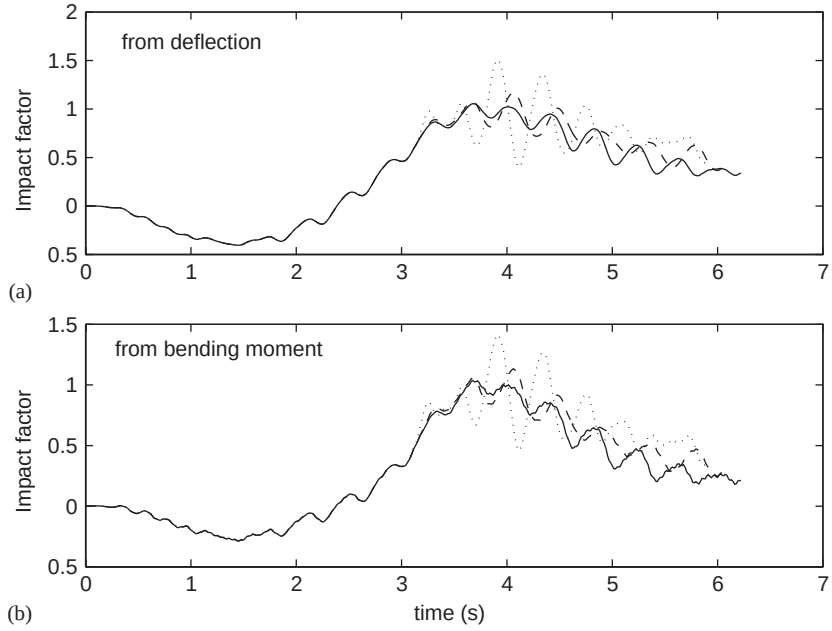

Fig. 8. Impact factor at middle of second span from different braking rise time and braking at $3/7L$ (— 0.6; - - - 0.3; ⋯ 0.0 s).

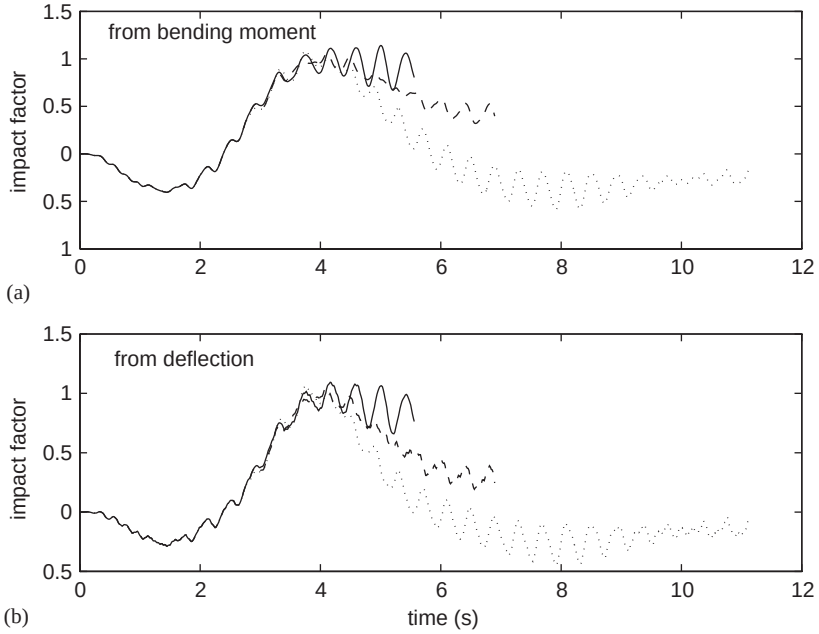

Fig. 9. Impact factor at middle of second span from different amplitude of braking force (— $0.6m_cg$; - - - $0.4m_cg$; ··· $0.2m_cg$).

Table 2
Impact factor from deflection and moment with different road surface conditions (three-span bridge deck)

Road class		Span	A	B	C	D	E
17 m/s no braking	Deflection impact factor	1	1.01	1.02	1.08	1.19	1.40
		2	1.02	1.05	1.11	1.24	1.50
		3	1.07	1.15	1.32	1.65	2.29
	Moment impact factor	1	1.05	1.06	1.12	1.24	1.45
		2	1.02	1.05	1.11	1.23	1.49
		3	1.11	1.20	1.37	1.71	2.33
1.7m/s no braking	Deflection impact factor	1	1.00	1.03	1.10	1.24	1.34
		2	1.02	1.08	1.15	1.30	1.59
		3	1.01	1.05	1.10	1.14	1.46
	Moment impact factor	1	1.04	1.06	1.11	1.25	1.35
		2	1.02	1.07	1.12	1.25	1.49
		3	1.04	1.08	1.12	1.17	1.46

braking force $F_{d\,\max}$ has a little effect on the maximum impact factor with the largest value of 1.14 for $F_{d\,\max}=0.6m_cg$. The corresponding interaction axle forces are shown in Fig. 10. The curves indicate approximately proportional increase in the interaction forces in the first and the third axles, while that in the second axle exhibits very small change with $F_{d\,\max}$. This phenomenon is due to the pitching action of the vehicle.

Table 3
Impact factor from deflection and moment in the second span with different braking position of vehicle on different classes of road

Road class		A	B	C	D	E
Brake at 1/7L	Deflection	0.43	0.45	0.51	0.69	1.05
	Moment	0.48	0.49	0.52	0.67	0.96
Brake at 2/7L	Deflection	1.03	1.04	1.10	1.24	1.65
	Moment	1.02	1.03	1.09	1.02	1.55
Brake at 3/7L	Deflection	1.03	1.06	1.12	1.26	1.50
	Moment	1.03	1.06	1.11	1.23	1.47
Brake at 4/7L	Deflection	1.02	1.05	1.11	1.24	1.50
	Moment	1.02	1.05	1.11	1.23	1.49
Brake at 5/7L	Deflection	1.02	1.05	1.11	1.24	1.50
	Moment	1.02	1.05	1.11	1.23	1.49
Brake at 6/7L	Deflection	1.02	1.05	1.11	1.24	1.50
	Moment	1.02	1.05	1.11	1.23	1.49

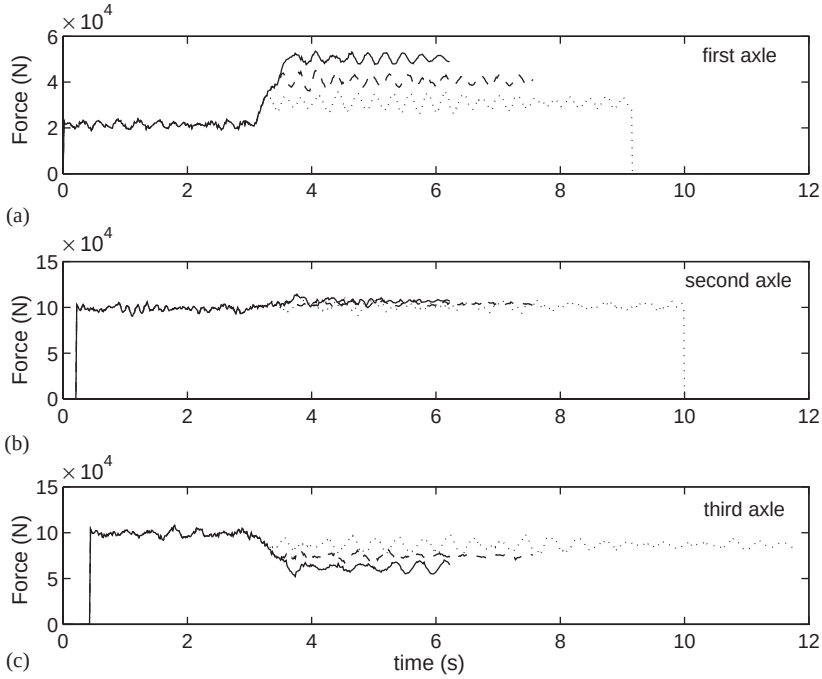

Fig. 10. Interaction axle forces from different amplitude of braking force (— $0.6\,m_c g$; - - - $0.4\,m_c g$; ⋯ $0.2\,m_c g$).

(e) Fig. 11 gives the maximum impact factors at the second span from different vehicle velocity and braking positions. The vehicle braking force $F_{d\,\max} = 0.6 m_c g$ and the braking rise time $t_b = 0.6$ s. Both factors have little effect on the impact factor when braking occurs at $1/7L$. This is because braking occurs at the first span and the vehicle never reaches the middle of the second

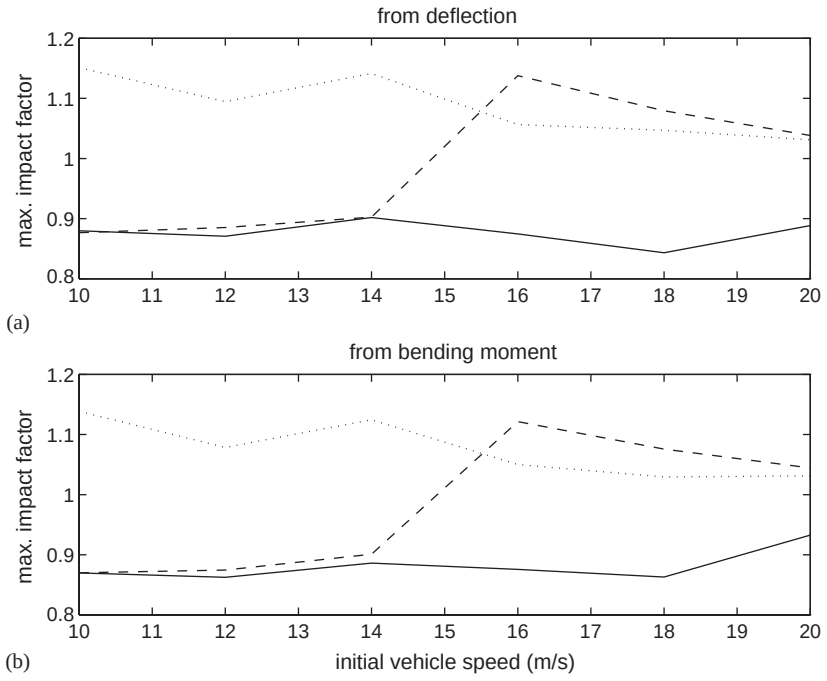

Fig. 11. Maximum impact factor from different initial vehicle speed and braking position (braking at: — $1/7L$; - - - $2/7L$; ⋯ $3/7L$).

span. When braking occurs at $3/7L$, all the impact factors are larger than unity, and it gradually decreases with higher velocity. The maximum is approximately 1.15 at 10 m/s velocity, the lower end of the velocity range. When braking occurs at $2/7L$, which is almost on top of the second support, it creates compression in the suspension system of the vehicle. And when it comes into the second span, the vehicle will bounce on top of the bridge deck causing higher impact factors than usual. However, their values are not higher than those obtained when braking at the most critical location of $3/7L$ as seen in Fig. 11.

(f) Table 2 shows the impact factor for different classes of roads. The impact factor increases with velocity very significantly only in the third span, and there is very small change in the other spans. Both bending moments and deflections give approximately the same impact factor. Since spans 1 and 3 are identical, this difference may be due to the different initial conditions of the vehicle at entry to the two spans (zero initial conditions for span 1 and non-zero conditions for span 3). This can also be found in Fig. 6 where the maximum impact factors are similar for both spans 1 and 3, but the impact factors here are larger due to the inclusion of road surface roughness in the analysis.

(g) Table 3 shows the impact factor for the case of $F_{d\,\max} = 0.6m_c g$, $t_b = 0.6$ s and 17 m/s initial velocity with braking at different locations. The maximum impact factor increases slightly with the road surface roughness in road Classes A–E, and the impact factor from deflection and moment are approximately the same for all Road Classes. Small impact factors are found when braking starts at $1/7L$ and the reason is as explained for Fig. 11. Those factors from

braking at $3/7L$ are largest, and those from braking beyond $3/7L$ are the same. This is similar to the observation for a single-span beam where braking within the first quarter span produces the most dynamic responses. A more correct definition of impact factor for a continuous beam is therefore needed from the above observations. The impact factor due to braking effect should be based on a comparison of the maximum dynamic and static responses at the same span in which braking occurs.

7. Experiments and results

The experimental setup has been reported previously [22] and is briefly described here for clarity on the test procedures. It is shown diagrammatically in Fig. 12. The main beam, 3678 mm long with a 100 mm × 25 mm uniform cross-section, is simply supported. There is a leading beam for accelerating the vehicle and a tailing beam to accept the vehicle when it comes out of the main span. A U-shaped aluminum section is glued to the upper surface of the beams as a direction guide for the car. The model car is pulled along the guide by a string wound around the drive wheel of an electric motor. Thirteen photoelectric sensors are mounted on the beams to measure and monitor the moving speed of the car. Seven strain gauges are evenly located on the beam to measure the bending moment responses of the beam. A TEAC 14-channels magnetic tape recorder and an 8-channel dynamic testing and analysis system are used for data collection and analysis in the experiment. The sampling frequency is 2000 Hz.The recorded length of each test lasts for 6 s. The model car has two axles at a space of 0.557 m and it runs on four steel wheels with rubber band on the outside. The mass of the whole car is 16.6 kg or 11.8 kg for the experiments

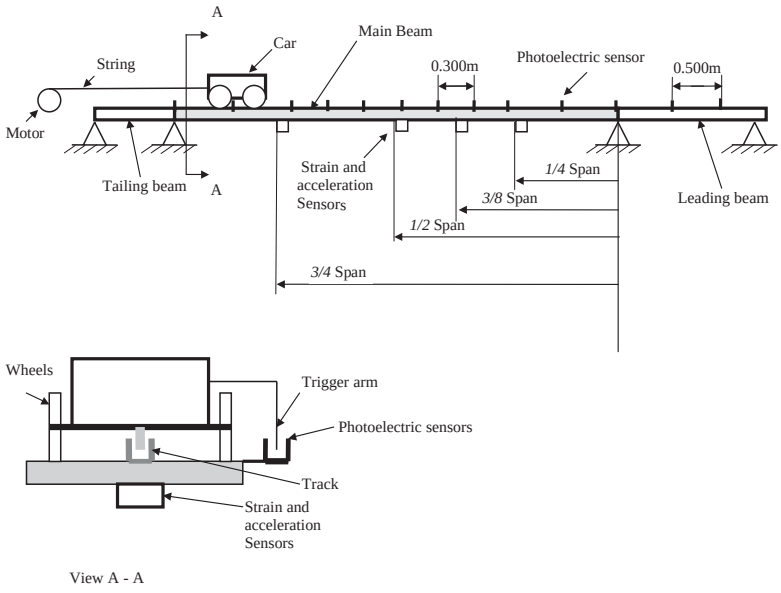

Fig. 12. Experimental setup of the bridge-vehicle system.

described below. The braking force was applied with a set of rubber bands between two fixed anchorage points. It was placed in front of the vehicle approximately at the level of its centroid, and the braking force was adjusted by adjusting the tension in the rubber band.

Since there is no distinct suspension system in the model car, the vertical stiffness K_c and the damping C_c are not considered, and the car is modeled as a rigid body moving on top of the beam. The beam sub-system has very small damping, and hence the damping stiffness C_b is set to zero in the computation. In the study with a two-span continuous beam, the same main beam is used with the intermediate support at 1.875 m from the left end.

7.1. Experiment on a single-span simply supported beam

A time step of 0.005 s is adopted in the integration of the responses in the solution of the equations of motion, and this covers the first six modes of the beam structure.

The first experiment is conducted with the mass of the car equals 16.6 kg. The vehicle speed is 1.22 m/s, and it brakes at 0.878 m from the left support. The car gets outside the main beam at the end of braking. Fig. 13 shows the measured and the calculated strains at $1/4L$, $1/2L$ and $3/4L$. The strains at each cross-section are very close to the measured ones indicating good estimates on the responses of the structure under the braking action of a moving vehicle using the proposed method. There is a slight under-estimation in the $1/4L$ strain when the vehicle moves away from the section, and there is a slight overestimation in the $3/4L$ strain when the vehicle moves towards the section. This is due to the gentle slope in the beam under its own weight that is not included in the formulation of the road surface roughness function.

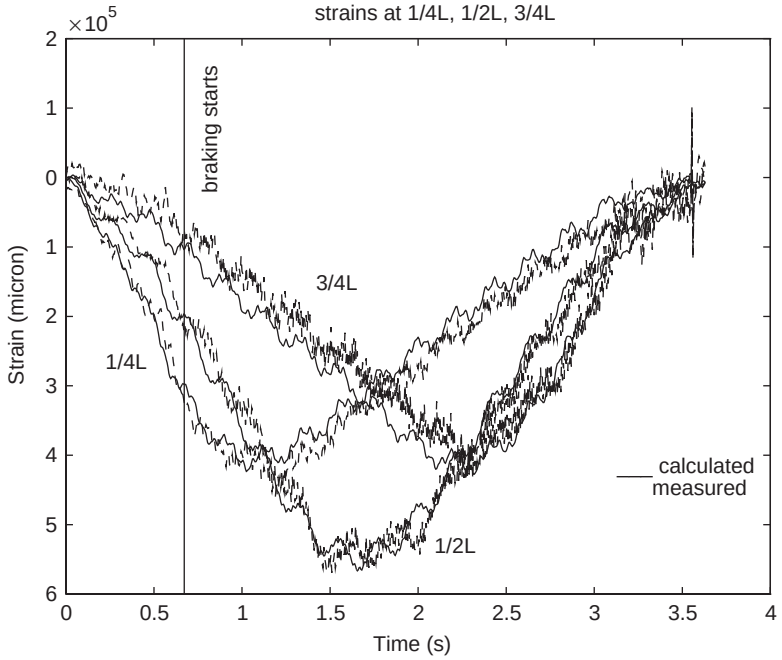

Fig. 13. Measured and calculated strains from gentle braking on single-span beam.

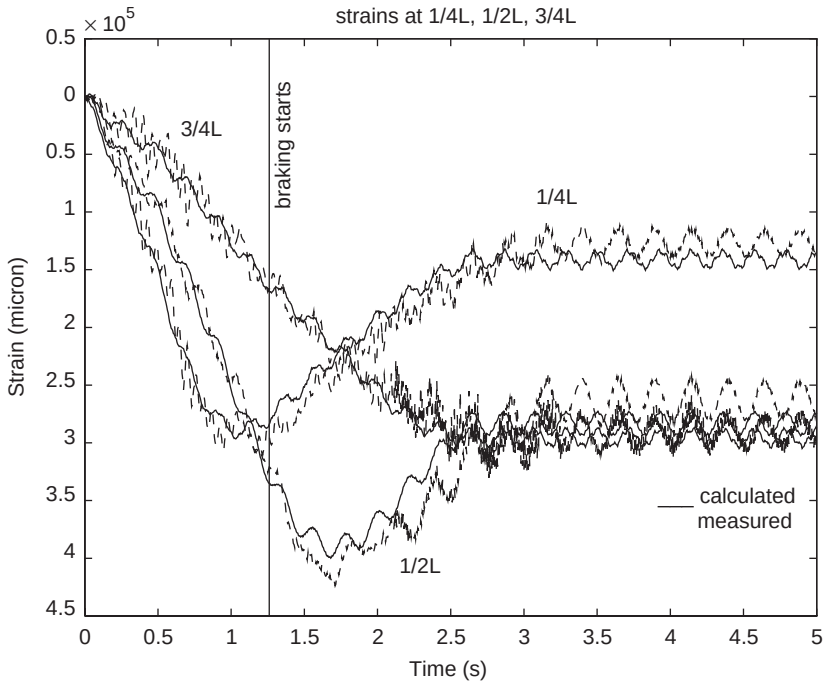

Fig. 14. Measured and calculated strains from hard braking on single-span beam.

The second experiment is conducted with a larger braking force. The vehicle speed is 1.12 m/s, and the mass of the whole car is 11.8 kg. It brakes at 1.4 m from the left support, and the car eventually stops on top of the beam. Fig. 14 shows the measured and the calculated strains. There is a large difference between the strains at $1/2L$ soon after braking. This is due to the pitching motion of the vehicle at braking which is equivalent to an application of an impulsive force on the beam causing large responses. The responses from the higher modes have not been included in the calculation. The large response forming the second mode of the beam is also absent at this location.

7.2. Experiment on a two-span continuous beam

A time step of 0.002 s is adopted in the integration of the responses in the solution of the equations of motion, and this covers the first five modes of the beam structure.

The third experiment is conducted with the mass of the whole car equals to 16.6 kg. The vehicle speed is 1.25 m/s, and it brakes at 0.878 m from the left support. The car stops outside the main beam. Fig. 15 shows a distinct periodic response in the $1/4L$ strain when the vehicle is on the first span. This response corresponds to the second mode of the beam, and it is believed to be the result of excitation by the unsteady motion of the vehicle. Similar large fluctuations in the $3/4L$ strain are also found when the vehicle is around the middle of the second span. The calculated strains vary close to the experimental values.

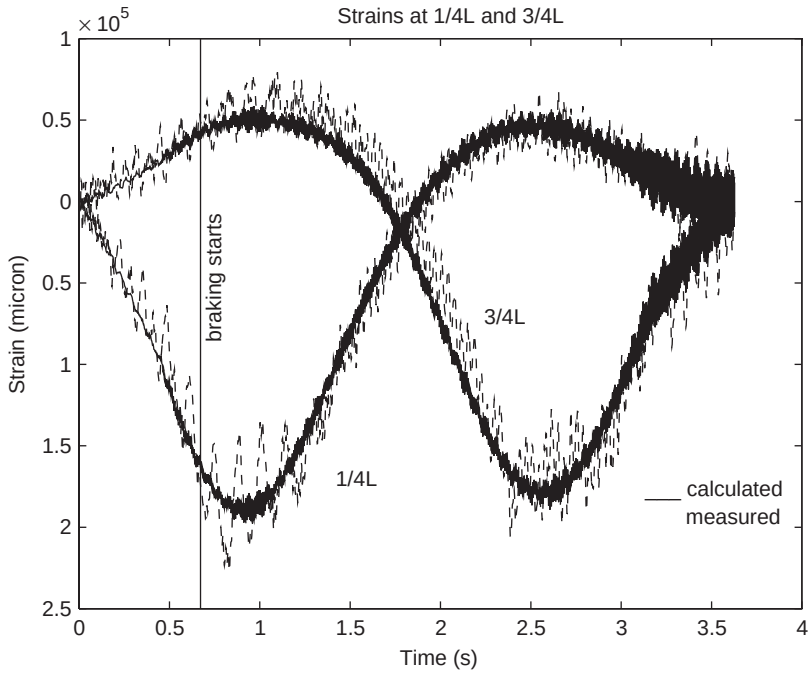

Fig. 15. Measured and calculated strains from gentle braking on the two-span beam.

The fourth experiment is conducted with a larger breaking force. The mass of the whole car is 11.8 kg. It moves at 1.75 m/s and it brakes at 1.4 m from the left support. The car eventually stops on top of the beam. Fig. 16 shows large fluctuations in the measured strains but with the mean very close to the calculated strains. This fluctuation in the strain response is due to the large pitching motion of the vehicle induced by the braking force from the rubber bands which are not placed at exactly the level of center of gravity of the vehicle, thus causing large and unsteady motion of the vehicle.

8. Conclusions

Numerical and experimental studies have been performed on the dynamic responses of simply supported single-span and two-span bridge decks modeled as Euler–Bernoulli beams. Several important observations have been made on the characteristics of the dynamic responses under a traveling vehicle modeled as a group of moving loads:

- Vehicle traveling at low speed over a very rough road surface may experience excitations at frequencies close to its own natural frequencies, generating large excitation force on the bridge deck and leading to larger dynamic response in the structure.
- The suspension system of the vehicle has a significant effect on the dynamic responses of the bridge deck under moving load, particularly with vehicle braking on top of the structure. The

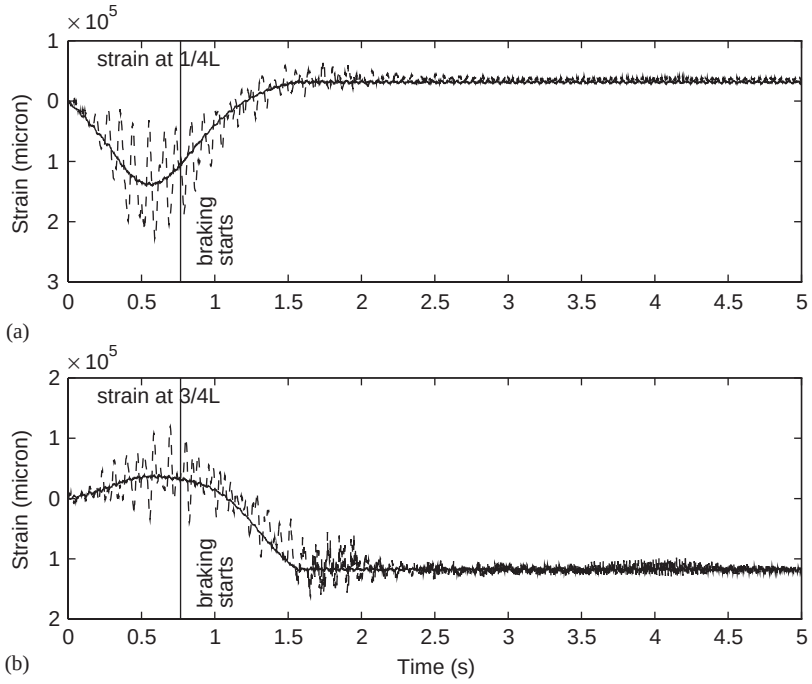

Fig. 16. Measured and calculated strains from hard braking on the two-span beam (— calculated; - - - measured).

pitching action of the vehicle during constant speed movement or braking creates large oscillations in the dynamic responses of the structure which are at the pitching frequency of the vehicle.

- For a multi-span bridge deck, the dynamic response is different for each span, and is smallest in the second span of the three-span bridge deck under study. This difference is larger in the case with braking of vehicle. A more correct definition of impact factor with vehicle braking should be based on a comparison of the maximum dynamic and static responses at the same span in which braking occurs.
- The dynamic response in the first span of a multi-span bridge is smaller than that in the other spans because of the smaller initial conditions of the vehicle at entry of the first span compared with those for the other spans.
- Vehicle braking generates an equivalent impulsive force covering a wide range of frequencies. A large number of vibration modes is required in the computation for a higher accuracy in the dynamic responses of the structure.

Acknowledgements

The work described in this paper was supported by a grant from the Hong Kong Polytechnic University Research Funding Project No. V653.

Appendix A

The equations of motion of the vertical motion of the vehicle-bridge system are

$$M_c\ddot{Y} + C_c\dot{Y} + K_c Y = F_c,$$
$$M_b\ddot{Q} + C_b\dot{Q} + K_b Q = F_b, \tag{11}$$

where

$$F_c = \Big\{-(m_1+m_2)b_1\ddot{\hat{x}}_1(t),\ (m_1+m_2)b_1\ddot{\hat{x}}_1(t),\ m_2b_2\ddot{\hat{x}}_1(t),$$
$$-P_1(t),\ -P_2(t),\ -P_3(t),\ -m_2b_2\ddot{\hat{x}}_1(t)\Big\}^{\mathrm{T}},$$
$$F_b = \left\{\sum_{s=1}^{3} W_i(\hat{x}_s(t))P_s'(t), i = 1,2,\ldots,n\right\},$$
$$P_1'(t) = P_1(t) + (m_1a_2 + m_2a_4a_6 + m_3)g,$$
$$P_2'(t) = P_2(t) + (m_1a_1 + m_2a_3a_6 + m_4)g,$$
$$P_3'(t) = P_3(t) + (m_2a_5 + m_5)g,$$

$$Y = \{y_1, y_2, \ldots, y_7\}^{\mathrm{T}},$$
$$Q = \{q_1(t), q_2(t), \ldots, q_n(t)\}^{\mathrm{T}},$$
$$M_b = \left\{\int_0^L \rho A(x)W_i(x)W_j(x)\,\mathrm{d}x\ (ij = 1,2,\ldots,n)\right\},$$
$$K_b = \left\{\int_0^L EI(x)W_i''(x)W_j''(x)\,\mathrm{d}x + k_s\sum_{l=1}^{R-1} W_i(x_l)W_j(x_l)\quad (i,j = 1,2,\ldots,n)\right\},$$
$$K_c = \begin{bmatrix} K_{c1} & -K_{c2} & K_{c3}^{\mathrm{T}} \\ -K_{c2} & K_{c2} & 0 \\ K_{c3} & 0 & K_{c4} \end{bmatrix},\quad M_c = \begin{bmatrix} M_{c1} & 0 & M_{c3}^{\mathrm{T}} \\ 0 & M_{c2} & 0 \\ M_{c3} & 0 & M_{c4} \end{bmatrix},$$

$$M_{c1} = \begin{bmatrix} m_1a_2^2 + \frac{J_1}{S_1^2} + (m_1+m_2)b_1^2 & m_1a_1a_2 - \frac{J_1}{S_1^2} - (m_1+m_2)b_1^2 & -m_2b_1b_2 \\ m_1a_1a_2 - \frac{J_1}{S_1^2} - (m_1+m_2)b_1^2 & m_1a_1^2 + \frac{J_1}{S_1^2} + (m_1+m_2)b_1^2 & m_2b_1b_2 \\ -m_2b_1b_2 & m_2b_1b_2 & m_2(a_5^2+b_2^2) + \frac{J_2}{S_2^2} \end{bmatrix},$$
$$M_{c2} = \mathrm{diag}(m_3, m_4, m_5),$$
$$M_{c3} = \begin{bmatrix} m_2b_1b_2 & -m_2b_1b_2 & m_2a_5a_6 - \dfrac{J_2}{S_2^2} - m_2b_2^2 \end{bmatrix},$$

$$M_{c4} = \left[m_2(a_6^2 + b_2^2) + \frac{J_2}{S_2^2} \right],$$

$$K_{c1} = \begin{bmatrix} k_1 + k_7 a_4^2 & k_7 a_3 a_4 & 0 \\ k_7 a_3 a_4 & k_2 + k_7 a_3^2 & 0 \\ 0 & 0 & k_3 \end{bmatrix},$$

$$K_{c2} = \mathrm{diag}(k_1, k_2, k_3, k_4),$$

$$K_{c3} = \begin{Bmatrix} -k_7 a_4 & -k_7 a_3 & 0 \end{Bmatrix},$$

$$K_{c4} = \{k_7\}.$$

References

[1] M. Fafard, M. Bennur, M. Savard, A general multi-axle vehicle model to study the bridge-vehicle interaction, *Engineering Computation* 14 (5) (1997) 491–508.

[2] T.L. Wang, D.Z. Huang, Cable-stayed bridge vibration due to road surface roughness, *Journal of Structural Engineering* 118 (5) (1992) 1354–1374.

[3] T.L. Wang, D.Z. Huang, M. Shahawy, Dynamic response of multi-girder bridges, *Journal of Structural Engineering* 118 (8) (1993) 2222–2238.

[4] D.Z. Huang, T.L. Huang, M. Shahawy, Impact studies of multi-girder concrete bridges, *Journal of Structural Engineering* 119 (21) (1993) 2387–2402.

[5] M. Fafard, M. Savard, M. Bennur, Dynamic analysis of existing continuous bridge, *Journal of Bridge Engineering* 3 (1) (1998) 28–37.

[6] K. Henchi, M. Fafardm, M. Talbot, G. Dhatt, An efficient algorithm for dynamic analysis of bridges under moving vehicles using a coupled modal and physical components approach, *Journal of Sound and Vibration* 212 (4) (1998) 663–683.

[7] J.W. Kou, J.T. DeWolf, Vibration behavior of continuous span highway bridge- influencing variables, *Journal of Structural Engineering* 123 (3) (1997) 333–344.

[8] K. Chompooming, M. Yener, The influence of roadway surface irregularities and vehicle deceleration on bridge dynamics using the method of lines, *Journal of Sound and Vibration* 183 (4) (1995) 567–589.

[9] P.K. Chatterjee, T.K. Datta, C.S. Surana, Vibration of continuous bridges under moving vehicles, *Journal of Sound and Vibration* 169 (5) (1994) 619–632.

[10] M.F. Green, D. Cebon, Dynamic interaction between heavy vehicles and highway bridges, *Computers and Structures* 62 (2) (1997) 253–264.

[11] S. Lu, X.J. Deng, Prediction vertical dynamic loads caused by vehicle-pavement interaction, *Journal of Transportation Engineering* 124 (5) (1998) 470–477.

[12] R.K. Gupta, R.W. Traill-Nash, Bridge dynamic loading due to road surface irregularities and braking of vehicle, *Earthquake Engineering and Structural Dynamics* 8 (1980) 83–96.

[13] M.F. Green, D. Cebon, D.J. Cole, Effects of vehicle suspension design on dynamics of highway bridges, *Journal of Structural Engineering* 121 (2) (1995) 272–282.

[14] N.L. Mulcahy, Bridge response with tractor-trailer vehicle loading, *Earthquake Engineering and Structural Dynamics* 11 (1983) 649–665.

[15] F. Yang, G.A. Fonder, An iterative solution method for dynamic response of bridge-vehicles systems, *Earthquake Engineering and Structural Dynamics* 25 (1996) 195–215.

[16] Y.B. Yang, B.H. Lin, Vehicle-bridge interaction analysis by dynamic condensation method, *Journal of Structural Engineering* 121 (11) (1995) 1636–1643.

[17] Y.B. Yang, J.D. Yau, Vehicle-bridge interaction element for dynamic analysis, *Journal of Structural Engineering* 123 (11) (1997) 1512–1518.
[18] H. Kishan, R.W. Traill-Nash, A modal method for calculation of highway bridge response with vehicle braking, *Institution of Engineers, Australian Civil Engineering Transactions* CE19 (1977) 44–50.
[19] R.K. Gupta, R.W. Traill-Nash, Vehicle braking on highway bridges, *Journal of Engineering Mechanics* 106 (4) (1980) 641–658.
[20] ISO 8608. Mechanical vibration—Road surface profiles—reporting of measured data, 1995(E).
[21] D.Y. Zheng, Y.K. Cheung, F.T.K. Au, Y.S. Cheng, Vibration of multi-span non-uniform beams under moving loads by using modified beam vibration functions, *Journal of Sound and Vibration* 212 (3) (1998) 455–467.
[22] X.Q. Zhu, S.S. Law, Moving forces identification on a multi-span continuous bridge, *Journal of Sound and Vibration* 228 (2) (1999) 377–396.